Odd-parity electronic multipolar ordering in URu$_2$Si$_2$: Conclusions from Si and Ru NMR measurements

S. Kambe,[1] Y. Tokunaga,[1] H. Sakai,[1] T. Hattori,[1] N. Higa,[1] T. D. Matsuda,[1,*] Y. Haga,[1] R. E. Walstedt,[2] and H. Harima[3]

[1]*Advanced Science Research Center, Japan Atomic Energy Agency, Tokai-mura, Ibaraki 319-1195, Japan*
[2]*Physics Department, The University of Michigan, Ann Arbor, Michigan 48109, USA*
[3]*Department of Physics, Kobe University, Nada-ku, Kobe 657-8501, Japan*

We report ^{29}Si and ^{101}Ru NMR measurements on high-quality, single-crystal URu$_2$Si$_2$ samples with a residual resistivity ratio RRR $\sim$ 70. Our results show that the Si and Ru sites exhibit fourfold electronic symmetry around the c axis in the hidden-order state. A previously observed twofold contribution of Si NMR linewidth is concluded to be due to extrinsic magnetic centers. Since the U and Si sites are aligned along the c axis, we conclude further that the electronic state shows fourfold symmetry around the U site below the hidden-order transition. From this observed local symmetry, possible space groups for the hidden-order state are $P4/nnc$ or $I4/m$, based on group theoretical considerations. Since the order vector is considered to be $Q = (001)$, the hidden-order state is then found to be $P4/nnc$ with rank 5 odd parity, i.e., electric dotriacontapolar order.

I. INTRODUCTION

The heavy fermion superconductor URu$_2$Si$_2$ undergoes a second order phase transition [1–3] at $T_0 \sim 17.5$ K. Since the order parameter of the transition has not ever been clearly identified, such order has been termed "hidden order" (HO) [4]. Identification of the hidden-order parameter is currently one of the challenging topics in condensed matter physics [5].

In order to specify the order parameter, it is critical to determine the crystalline and electronic space group of the HO state, which have not yet been specified. The space group of the disordered (paramagnetic) state of URu$_2$Si$_2$ is No. 139 ($I4/mmm$). Based on Landau's theory of second order phase transitions [6], possible electronic space groups may be selected for the HO state [7]. The electronic space group for the HO state can be different from the crystalline space group.

In order to specify the electronic space group, it would be quite effective to determine the electronic (point) symmetry at local (U, Ru, and Si) sites. However, the local symmetry at the Ru and Si sites in the HO state is highly controversial. Magnetic torque, cyclotron resonance, elastoresistance, and XRD measurements all indicated twofold symmetry [8–11]. In contrast, the elastic constant, recent XRD, and thermal expansion measurements indicate fourfold symmetry [12–14]. Ru nuclear quadrupole resonance (NQR) reveals directly the local electronic symmetry, indicating fourfold symmetry at the Ru site in the HO state [15–17]. Previous Si nuclear magnetic resonance (NMR) data indicated a distributed twofold linewidth in the HO state. However, the intrinsic nature of this result could not be confirmed [18,19], and was, in fact, called into question [20].

In order to determine the intrinsic rotational symmetry, Si NMR spin-echo decay has been measured on a high-purity, single crystal URu$_2$Si$_2$ sample in the present study. The intrinsic electronic fourfold symmetry at the Si site is confirmed by these new measurements. This leads, in turn, to a conclusion of electronic fourfold symmetry at the U site in the HO state. The previously reported, distributed twofold Si NMR linewidth is considered to be caused by extrinsic magnetic broadening centers (MBCs) [20]. As a consequence, the two-domain explanation for the twofold linewidth [18,19] seems to be unlikely. In addition, the fourfold symmetry at the Ru site has been reconfirmed by ^{101}Ru NQR study on the same single-crystal sample. Based on these results, possible space groups and order parameters of URu$_2$Si$_2$ in the HO state are discussed in Sec. VI below.

II. EXPERIMENT

Single crystals were grown using the Czochralski method in a tetra-arc furnace under argon gas [21]. For NMR, we employed a single crystal sample having a nearly perfect cylindrical shape (1 mm $\phi \perp [001] \times 3$ mm $\parallel [001]$), with narrow facets on the (110) planes. This sample has been used in previous studies [18–20]. Since the cross section of the sample through the (001) (i.e., basal) plane is nearly a perfect circle, demagnetization effects are very nearly independent of field direction in the basal plane. Any variation of demagnetization fields should be much less than $\sim$1 Oe (i.e., $\sim$0.85 kHz for ^{29}Si NMR), since an estimated demagnetization field is $\sim$1 Oe for a 1 T applied field. In addition, the effective sample volume is small, since the skin depth of rf fields is $\sim$40 μm in the present measurements. Therefore, no distribution of demagnetization distortion of the line shape needs to be considered in the present case.

For the experimental crystal high sample purity was confirmed by a residual resistivity of $\sim$5 $\mu\Omega$ cm (RRR $\equiv$ $\rho(300$ K$)/\rho(2$ K$) \sim 70$). Resistivity was measured on a piece cut ($2 \times 0.5 \times 0.5$ mm^3) from the same single crystal used

for NMR measurements. No trace of ferromagnetic or anti-ferromagnetic long-range order was detected down to 2 K. It should be noted that URu_2Si_2 single crystals with RRR > 50 are already high quality single crystals in the usual sense [21].

The natural abundance of the NMR isotope ^{29}Si ($I = 1/2$, gyromagnetic ratio $\gamma/2\pi = 0.84577$ kHz/Oe) is only 4.7%. In order to obtain highly accurate spin-echo decay results in the present study, a single crystal sample with a concentration $c = 53\%$ enriched ^{29}Si isotope has been prepared, improving the NMR sensitivity by a factor $\sim$11. As there are no quadrupolar interactions for $I = 1/2$ nuclei, ^{29}Si NMR spectra reflect only magnetic shift and broadening effects.

A standard pulsed NMR spectrometer was used, with magnetic field provided by a 12 T superconducting magnet in the persistent mode. The applied magnetic field is precisely rotated in the basal plane using a two-axis rotational stage for the sample mount. NMR spectra were obtained using fast Fourier transformation (FFT) of spin-echo signals at a fixed applied magnetic field. Using a standard $\pi/2$-π pulse sequence, the spin-echo amplitude $m(2\tau)$ so generated was measured as a function of the time τ between pulses to record the spin-echo decay. Here a typical $\pi/2$ pulse width was 4–5 μs. Since the resonance linewidth is rather narrow (e.g., $\sim$2 kHz at 2.6 T), all nuclear spins in the spectrum were quite uniformly excited by the rf pulses used. The pulse repetition time t_{rep} was adjusted to be much longer than the previously determined spin-lattice relaxation time T_1 [22,23].

^{101}Ru ($I = 5/2$) NQR under zero field was measured in the same single-crystal sample using the same spectrometer. ^{101}Ru NQR spectra were obtained using FFT of the spin-echo signal in order to determine the central NQR frequency.

III. SILICON NMR MEASUREMENTS

In this section we use the ^{29}Si NMR spin-echo decay to examine the local symmetry of the Si site. A detailed description of the spin-echo decay and nuclear spin-spin interactions was published earlier [24,25]. We note that the situation for the ^{29}Si NMR spin-echo decay is very similar to that in $YbRh_2Si_2$, for which a previous analysis was also published [24].

A. Spin-echo decay and homogeneous and inhomogeneous broadenings

The ^{29}Si homogeneous line broadening in URu_2Si_2 is somewhat complex, with local spin-spin interactions consisting of Ruderman-Kittel (RK) indirect exchange [26] via conduction electrons as well as Bloembergen-Rowland pseudodipolar (PD) coupling [27] along with the classical dipolar coupling that is always present. These three contributions make up the intrinsic, microscopic broadening factors, which are expected to reflect the local electronic symmetry of the Si site.

Accordingly, the ^{29}Si nuclear spin Hamiltonian is given by

$$\mathcal{H}_{NMR} = \frac{1}{2}\sum_{i \neq j}[J_{ij} + B_{ij}]\vec{I}_i \cdot \vec{I}_j - \frac{3}{2}\sum_{i \neq j}B_{ij}I_{zi}I_{zj}, \quad (1)$$

where $B_{ij} = \frac{1}{2}[b_{ij} + \gamma^2\hbar/r_{ij}^3](3\cos^2\Omega_{ij} - 1)$. Here b_{ij} is a coefficient representing the PD coupling term [27], $\gamma^2\hbar/r_{ij}^3$ is the classical dipole coupling term, J_{ij} represents the RK interaction [26], Ω_{ij} represents the angle between the applied

field, and the radius vector $\vec{r}_{ij}$ between ^{29}Si sites "i" and "j". In general, Eq. (1) presents a highly complex set of behaviors, with fluctuation terms and even the possibility of exchange narrowing of the echo decay function. For URu_2Si_2 and $YbRh_2Si_2$ [24], however, there are special circumstances that greatly simplify the behavior of the ^{29}Si spin-echo decay. In our crystals of these compounds the ^{29}Si NMR lines are found to have inhomogeneous broadening from local disorder that is much greater than any spectral widths stemming from $\mathcal{H}_{NMR}$. Furthermore, the resulting inhomogeneity is local in character, so that the $I_{+i}I_{-j} + I_{-i}I_{+j}$ terms are rendered inert and thus nonsecular (see the Appendix). As a result, the foregoing flip-flop terms in $\mathcal{H}_{NMR}$ may be disregarded in the following linewidth calculations (see also similar results for $YbRh_2Si_2$ [24]).

Thus, keeping only the $I_{zi}I_{zj}$ terms, $\mathcal{H}_{NMR}$ is then truncated to give

$$\mathcal{H}_{Tr} = \frac{1}{2}\sum_{i \neq j}I_{zi}I_{zj}[J_{ij} - 2B_{ij}]. \quad (2)$$

Note that this "homogeneous" broadening Hamiltonian is entirely static in character in URu_2Si_2. As a result, when the rephasing pulse angle is small, T_{2G} becomes very long. Thus, any genuinely dynamic nuclear spin fluctuations are very weak. In such a case, the echo is relaxed entirely through the reorientation of neighbor spins by the refocusing (second) pulse [28]. This confirms that the echo oscillations are not affected by other dynamical fluctuations, even T_1, which is much longer than the observed T_{2G}. Spin-echo decay data illustrating this point for the ^{29}Si spins in the crystal used for this investigation are shown and discussed in the Appendix.

As noted above, the ^{29}Si NMR line is broadened by what are evidently local static inhomogeneities caused by defects in the crystal, in addition to the homogeneous broadening. This type of broadening seems to be an almost inherent property of high-quality crystals of both URu_2Si_2 and $YbRh_2Si_2$ [24]. the resulting broadening effects have been studied in considerable detail [20]. Thus, as illustrated in Fig. 1, the linewidth is dominated by static inhomogeneous broadening, where the smaller effective width due to the homogeneous terms in Eq. (2) is represented by the dashed-line spectra (examples). The dashed-line spectrum does not really reside at any particular point within the inhomogeneous envelope, because the corresponding echo decay form that we model here could be observed at any point within the broader curve.

The spin-echo formation process is illustrated in Fig. 2 with a $\pi/2$-π excitation pulse sequence followed by the echo at time 2τ. The inhomogeneous Lorentzian spectrum illustrated in Fig. 1 is the FFT of echo profile in time. The echo width in the case at hand is small compared with its decay time.

As shown in Fig. 3, indeed a typical homogeneous Gaussian linewidth is much smaller than the inhomogeneous Lorentzian linewidth in the HO state of URu_2Si_2. In Sec. V we discuss the findings reported for the inhomogeneous broadening effect, which are an important story by themselves.

Taking up the decay problem, we note that a complete analysis of spin-echo decay resulting from the terms in Eq. (1) was published many years ago by Alloul and Froidevaux [29]. We quote here the result from that paper which applies to the
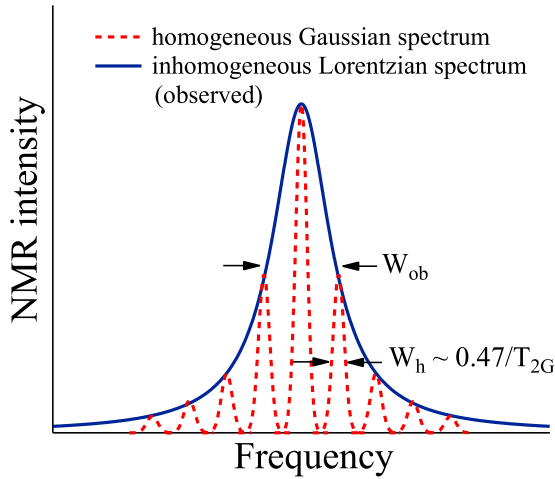
FIG. 1. Figure showing the overarching static broadening curve (solid line), within which one may observe an echo decay curve determined by homogeneous broadening represented by the broken line. Such a decay curve could be traced out anywhere within the broad profile. In practice we excite the entire static distribution of ^{29}Si nuclear spins. The full widths at half maximum W_h and W_{ob} are defined as indicated.

static case of Eq. (2), namely [24],

$$m(2\tau) = m(0)\langle \Pi_k \cos(\tilde{J}_{0k}\tau)\rangle_{av}, \tag{3}$$

where $\tilde{J}_{0k} = J_{0k} - [b_{0k} + \gamma^2\hbar/r_{0k}^3](3\cos^2\Omega_{0k} - 1)$ in terms of the parameters defined above. Here the indicated product is over all occupied Si neighbor sites labeled by k to the reference "0" site at the origin. The brackets indicate an ensemble average over all configurations of ^{29}Si neighbors at an occupation probability of c. Within the assumption of complete local detuning of neighboring ^{29}Si nuclear spins so that $I_{\mp i}I_{\pm j}$ operators are nonsecular, Eq. (3) is an *exact* result. What is inexact is our knowledge of the $\tilde{J}_{0k}$ parameters.

B. Echo decay function and RK interaction for URu$_2$Si$_2$

As shown in Fig. 4, the Si sites are arranged in nearest-neighbor (nn) pairs, which are only $|\vec{r}_{nn}| = 2.35$ Å apart in the crystal structure of URu$_2$Si$_2$. There are 12 more neighbor sites at distances between ~4 and 5 Å. Thus we expect the dominant nn pairs to yield an oscillation in the echo decay, while the more distant ^{29}Si would combine to produce a monotonic decay function. To the extent that more distant
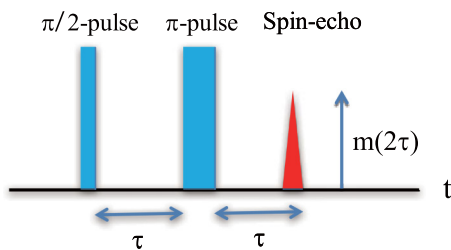

FIG. 2. Schematic description of NMR spin-echo formation. A $\pi/2$ pulse rotates the nuclear magnetic moment by 90°, a π pulse by 180°. As 2τ increases, $m(2\tau)$ decays owing to nuclear spin-spin interactions.
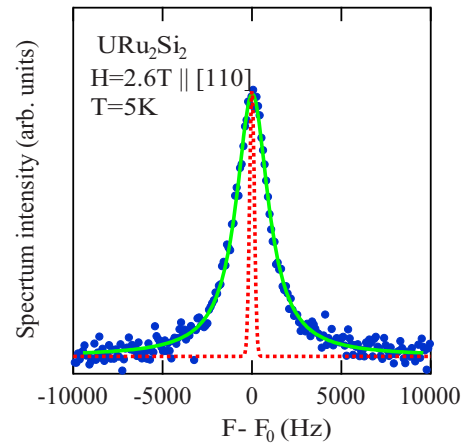

FIG. 3. Typical comparison between inhomogeneous Lorentzian (filled circles) spectrum obtained from FFT of spin-echo profile and homogeneous Gauss spectrum (dashed line) obtained from Fourier transformation of nonoscillating part of spin-echo decay $m(2\tau)/m(0)$ [i.e., the first term of Eq. (11), see below] in the HO state of URu$_2$Si$_2$. Solid line is fitted curve using the Lorentzian function. Here F_0 corresponds to the ^{29}Si NMR resonance frequency at 2.6 T (i.e., ~22 MHz). FWHM of Lorentzian and Gaussian spectra corresponds to W_{ob} and W_h, respectively.

neighbors constitute randomly oriented and distributed sources of local field, the central limit theorem suggests that they will produce an essentially Gaussian decay profile. Such a picture was found to be very nearly correct for the nearly identical case of YbRh$_2$Si$_2$ [24]. The spin-echo decay profile given by Eq. (3) in this approximation can be written with a single oscillation term $\cos\{G(\theta)\tau\}$,

$$\frac{m(2\tau)}{m(0)} = \exp\left\{-\frac{2\tau}{T_1} - \frac{1}{2}\left(\frac{2\tau}{T_{2G}}\right)^2\right\}$$
$$\times [(1 - f_{osc}) + f_{osc}\cos\{G(\theta)\tau\}], \tag{4}$$

where $1/T_1$ is the spin-lattice relaxation rate, $1/T_{2G}$ is the Gaussian spin-spin relaxation rate, and f_{osc} is approximately the ^{29}Si concentration c. If the second-nn terms were
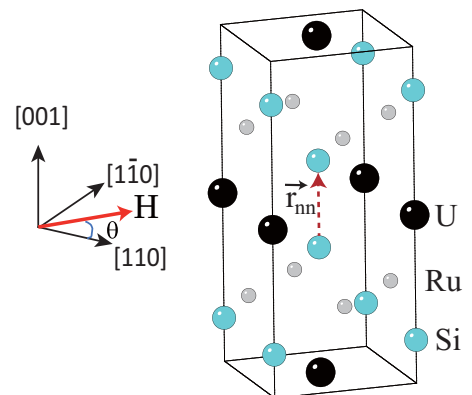

FIG. 4. Left: Definition of the angle θ between applied magnetic field H in the basal plane and the [110] direction. Right: Crystal structure of URu$_2$Si$_2$. The nn Si sites along the [001] axis are connected by a dashed arrow, which corresponds to $\vec{r}_{nn}$ ($|\vec{r}_{nn}| = 2.35$ Å) perpendicular to the basal plane.
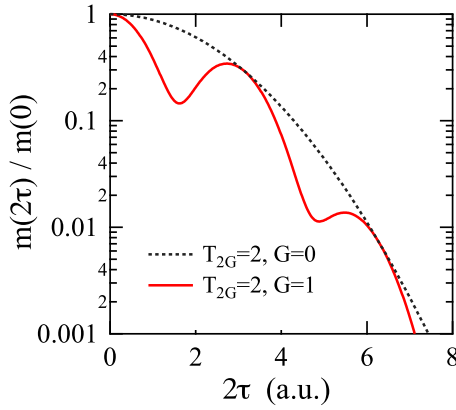
FIG. 5. Schematic spin-echo decay curves [Eq. (11)] for $c = 1/2$. Dotted line: Gaussian decay curve (i.e., $G = 0$) reflecting only T_{2G}. Solid line: The indirect interaction G causes an oscillating modulation of the Gaussian decay envelope.

contributing to the oscillation, there would be multiple oscillation terms [25]. G then becomes,

$$G \equiv \left| J - \left[b + \gamma^2 \hbar / r_{nn}^3 \right] (3 \cos^2 \Omega_{01} - 1) \right|, \quad (5)$$

where J_{0k} and b_{0k} are denoted J and b are for the nn site, respectively. In Fig. 5 the oscillating line shows a schematic decay function for $c = 1/2$ in Eq. (4), where the Gaussian decay envelope is shown as a dotted line. We note that W_h, the linewidth parameter corresponding to the Fourier transform of the Gaussian decay envelope, may be written

$$W_h \equiv \{\ln(2)/\pi\}^{1/2} \frac{1}{T_{2G}} = \frac{0.470}{T_{2G}}, \quad (6)$$

which is illustrated in Fig. 1.

Next, we discuss the nuclear spin-spin interactions G [Eq. (5)] in URu2Si2. For field orientations in the basal plane, we have $\Omega_{01} = 90°$ (see Fig. 4) so that Eq. (5) gives

$$G = \left| J + b + \gamma^2 \hbar / r_{nn}^3 \right|. \quad (7)$$

Thus, G is independent of field angle θ in the basal plane in the frame of original calculations [26,27], as expected for the nn sites in URu2Si2.

However, White [30] has shown that J, and presumably b, are related to wave-vector $\vec{q}$ summation of the θ-dependent static spin susceptibility $\chi_{\text{spin}}(\vec{q}, \theta)$ for direction of H defined in Fig. 4, so that J and b could be θ dependent in the case of anisotropic $\chi_{\text{spin}}(\vec{q}, \theta)$. Thus,

$$J(\theta), b(\theta) \propto \frac{j^2}{g_N g_e \mu_B^2} \sum_{\vec{q}} \chi_{\text{spin}}(\vec{q}, \theta) \exp[i \vec{q} \cdot \vec{r}_{nn}], \quad (8)$$

where j is the hyperfine interaction between nuclei and conduction electrons, and g_N and g_e are the nuclear and electronic g factors, respectively. Thus, G would reflect the fourfold symmetry of $\chi_{\text{spin}}(\vec{q}, \theta)$, as is realized in URu2Si2, yielding,

$$G(\theta) = G_1(T) + G_2(T) \cos 4\theta, \quad (9)$$

where $G_1(T)$ and $G_2(T)$ are T-dependent quantities. In addition, W_h would show fourfold symmetry, owing to fourfold

second moments having the same origin. Thus,

$$W_h(\theta) = W_{h1}(T) + W_{h2}(T) \cos 4\theta, \quad (10)$$

where $W_{h1}(T)$ and $W_{h2}(T)$ are T-dependent quantities. Note that the hyperfine coupling interaction appears to be almost isotropic in the basal plane [18], though g_e can show a slight fourfold anisotropy [31] which cannot be separated from fourfold anisotropy of $\chi_{\text{spin}}(\vec{q}, \theta)$ in the present study.

Finally, the spin-echo decay function in URu2Si2 is expressed in terms of $W_h(\theta)$ and $G(\theta)$ as

$$\frac{m(2\tau)}{m(0)} \approx \exp\left\{ -\frac{1}{2} \left(\frac{2\tau W_h(\theta)}{0.47} \right)^2 \right\}$$
$$\times [(1 - f_{\text{osc}}) + f_{\text{osc}} \cos\{G(\theta)\tau\}]. \quad (11)$$

The exponential decay factor $1/T_1$ in Eq. (4) is essentially negligible below 25 K in URu2Si2, because $1/T_{2G} \gg 1/T_1$. Below, we fit this decay profile form to experimental data on ^{29}Si in URu2Si2.

C. Experimental results for T_{2G} and G

Figure 6 shows spin-echo decay curves at 25 and 5 K for $H(\theta = 0)$, i.e., $H \parallel [110]$ in the single crystal sample with RRR ~ 70. The spin-echo decay curves are remarkably well fitted using Eq. (11), indicating that the nn sites dominate the oscillatory spin-echo decay and that the Gaussian approximation to the collective effect of more distant neighbors is very good, indeed. The spin-echo decay is independent of applied magnetic field up to 7 T, indicating that W_h is independent of applied field in contrast with W_{ob}, which increases with increasing field [19]. In addition, W_h is almost the same for samples with RRR > 40, indicating that W_h is insensitive to the sample quality for high RRR samples, as well as the other properties [21].

In the paramagnetic state we find $f_{\text{osc}} \simeq c$. In contrast, f_{osc} is slightly smaller than c in the HO state, and thus, the oscillation is slightly less pronounced in the HO state. This means that the effective number of ^{29}Si is decreased, owing perhaps to inhomogeneity in the HO state. Meanwhile, G is slightly decreased in the HO state, while W_h is slightly greater (see Figs. 6 and 7), suggesting that the phase and/or wavelength of RK oscillations are modified by the ordering process, perhaps due to modifications of Fermi surfaces.

Figures 7 and 8 show the θ dependence of G and W_h (i.e., $0.47/T_{2G}$), respectively, at 25 and 5 K, showing a clear fourfold dependence in the basal plane, which is well fitted by Eqs. (9) and (10): $G_1(5\,\text{K}) = 523\,\text{s}^{-1}$, $G_2(5\,\text{K}) = 33.9\,\text{s}^{-1}$, $G_1(25\,\text{K}) = 593\,\text{s}^{-1}$, $G_2(25\,\text{K}) = 20.5\,\text{s}^{-1}$, $W_{h1}(5\,\text{K}) = 349\,\text{s}^{-1}$, $W_{h2}(5\,\text{K}) = 34.9\,\text{s}^{-1}$, $W_{h1}(25\,\text{K}) = 312\,\text{s}^{-1}$, $W_{h2}(25\,\text{K}) = 41.2\,\text{s}^{-1}$. Since G and W_h are determined by the local electronic state at the Si sites, the observed fourfold dependence indicates that the electronic local symmetry of the Si site is fourfold rotational (C_4) in both the paramagnetic and HO states, in addition to the fourfold crystalline spatial symmetry indicated in XRD measurements [12].

The origin of the fourfold variation of G may be related with fourfold $\chi_{\text{spin}}(\vec{q})$ as given by Eq. (8). Although a fourfold total $\chi(0)$ has been reported [8], the spin contribution to that is still unclear. In addition, the $\vec{q}$ dependence of $\chi_{\text{spin}}(\vec{q})$ is
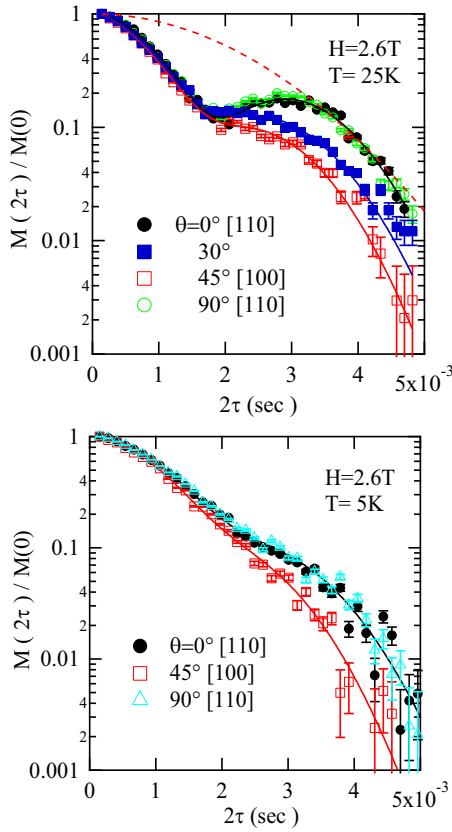
FIG. 6. Field angle dependence of spin-echo decay curves in the paramagnetic ($T = 25$ K) and HO ($T = 5$ K) states. Results at $\theta = 0°$ and $90°$ coincide with one another, indicating that fourfold symmetry is confirmed. Solid curves are least-squares fits using Eq. (11). The dashed line shows the fitted Gaussian decay envelope for $\theta = 0°$ at 25 K.

unknown. Thus, a quantitative comparison between the present results and $\chi_{spin}(\vec{q})$ is not yet available. In URu$_2$Si$_2$, a large anisotropy of $\chi_{spin}(0)$ between $H \parallel$ and $\perp [001]$ has been pointed out [32,33]. In addition to that, the present results
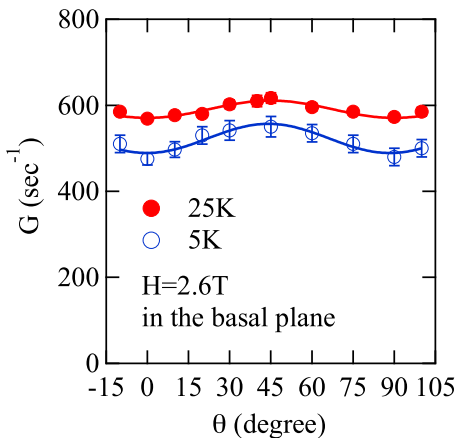

FIG. 7. Angle θ dependence of G in the paramagnetic (25 K) and HO (5 K) states. Solid curves are obtained by fittings using Eq. (9), i.e., $G(\theta) = 523 + 33.9\cos4\theta$ for 5 K; $G(\theta) = 593 + 20.5\cos4\theta$ for 25 K.
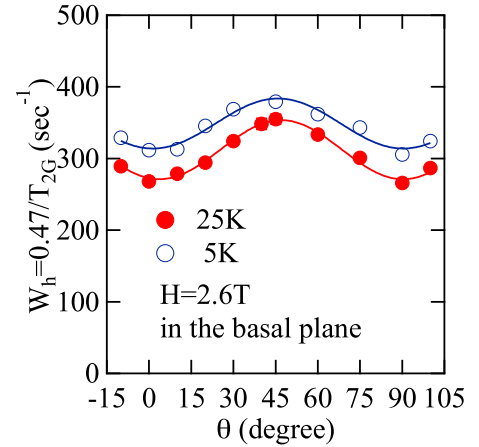

FIG. 8. θ dependence of $W_h = 0.47/T_{2G}$ in the paramagnetic (25 K) and HO (5 K) states. Solid curves are obtained by fits using Eq. (10), i.e., $W_h(\theta) = 349 + 34.9\cos4\theta$ for 5 K; $W_h(\theta) = 312 + 41.2\cos4\theta$ for 25 K.

indicate that $\chi_{spin}(\vec{q})$ has weak fourfold anisotropy in the basal plane. To our knowledge, this is the first observation of anisotropy for $\chi_{spin}(\vec{q})$ via NMR spin-echo decay measurements, a consequence of the very high sample quality.

It should be noted that the previously observed θ-independent ^{29}Si Knight shift determined at the peak position of Lorentzian spectra [18] is consistent with the fourfold symmetry of G, W_h, and $\chi_{spin}(\vec{q},\theta)$.

Figure 9 shows the T dependence of W_h for $H \parallel [110]$ and [100]. There are maxima of W_h in the HO state for both cases, indicating that the HO enhances W_h. However, the T dependence obtained in the HO state is peculiar, indicating that W_h does not simply reflect the T dependence of the order parameter. This peculiar T dependence is similar to that of W_{ob} for the $H \parallel [110]$, [100], and [001] directions reported previously [19,34].

As previously reported, the observed total static ^{29}Si-NMR linewidth W_{ob} shows a twofold character [18–20]. The total linewidth W_{ob} is much larger than W_h owing to inhomogeneity

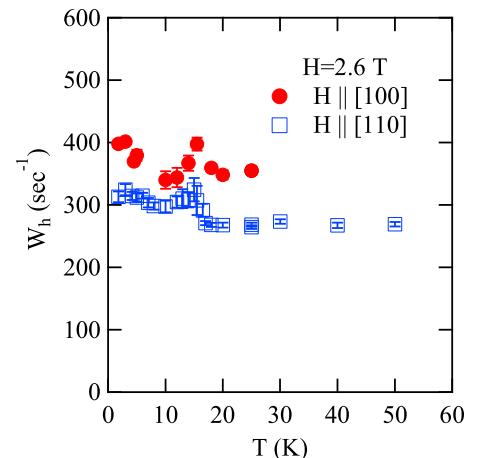FIG. 9. T dependence of W_h for $H \parallel [110]$ ($\theta = 0°$) and $H \parallel [100]$ ($\theta = 45°$). Peaks are shown at the HO transition $T_0 \sim 17.5$ K. There is a similarity between the T dependence of W_h and W_{ob} [19,34].
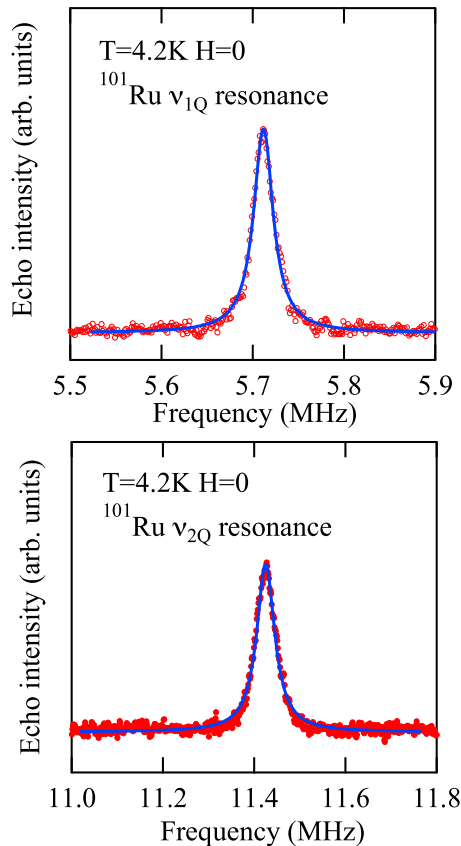
FIG. 10. ^{101}Ru NQR spectra at 4.2 K under zero field. Two resonance spectra: ν_{1Q} ($I = \pm 3/2 \leftrightarrow I = \pm 1/2$) and ν_{2Q} ($I = \pm 5/2 \leftrightarrow I = \pm 3/2$) have been observed. Solid lines are Lorentzian curves fitted to obtain values for ν_{1Q} and ν_{2Q}.

of the crystal lattice, e.g., defects and impurities. The observed fourfold W_h and twofold W_{ob} mean that the Si site is locally fourfold, but twofold character appears in the inhomogeneous broadening. The present fourfold spin-echo results indicate that the twofold character may be an extrinsic property. In Sec. V we discuss this effect in more detail.

IV. RUTHENIUM NQR MEASUREMENTS

In this section we describe Ru NQR measurements at zero field in the same single crystal sample to examine the electronic local symmetry of the Ru site. For ^{101}Ru ($I = 5/2$), two NQR resonances ν_{1Q} ($I = \pm 3/2 \leftrightarrow I = \pm 1/2$) and ν_{2Q} ($I = \pm 5/2 \leftrightarrow I = \pm 3/2$) have been observed. The ν_{1Q} frequency is related to the ν_{2Q} frequency in the case of an axial symmetry parameter $\eta \ll 1$ by [35]

$$\frac{\nu_{2Q}}{\nu_{1Q}} \cong 2\left(1 - \frac{35}{27}\eta^2\right). \tag{12}$$

If the fourfold local symmetry at the Ru site is not broken in the HO state, the axial parameter η should be zero.

Figure 10 shows ^{101}Ru NQR spectra in the HO state at 4.2 K. In the present measurements, $\nu_{2Q} = 11.425 \pm 0.002$ and $\nu_{1Q} = 5.712 \pm 0.001$. Thus, $\nu_{2Q}/\nu_{1Q} = 2.0002 \pm 0.0003$ is obtained, yielding $\eta = 0$ within experimental error in the HO state as well as in the paramag-

netic state ($\nu_{2Q} = 11.475 \pm 0.002$, $\nu_{1Q} = 5.737 \pm 0.001$, and $\nu_{2Q}/\nu_{1Q} = 2.0002 \pm 0.0003$ at 23 K in the present sample). This observation confirms previous results [15,16] for η at the Ru site in the present high-purity sample. Since the NQR frequencies reflect the electron distribution around the Ru nuclei through the electric field gradient [35], this observation confirms that the electronic local symmetry at the Ru site remains rotationally fourfold (S_4) in the HO state.

V. HOMOGENEOUS FOURFOLD AND INHOMOGENEOUS TWOFOLD LINE BROADENING

A. Twofold inhomogeneous linewidth due to crystal imperfections

Figure 11 shows the observed ^{29}Si NMR linewidth W_{ob} previously presented [18–20], together with the estimated homogeneous linewidth $W_h = 0.47/T_{2G}$. W_{ob} is considerably larger than W_h owing to the contributions of impurities and defects. Remarkably, the θ dependence of W_{ob} is orthogonal to that of W_h, indicating that the sources of θ dependence in W_{ob} and W_h are different from one another. As discussed previously, the $|\cos 2\theta|$ dependence of W_{ob} that occurs in the HO state appears to reflect distributed twofold magnetic broadening centers (MBC) [20], whereas W_{ob} shows only $\cos 4\theta$ dependence in the paramagnetic state.

The MBC model for twofold Lorentzian line broadening is expounded in [20], using a conventional theory of dilute RKKY broadening effects [36]. This model leads to an estimate of $\sim 1\%$ for the concentration of MBCs responsible for the twofold linewidth in the crystal used for these studies. Substantially higher MBC concentrations would very likely lead to deviations from a Lorentzian line shape. The twofold
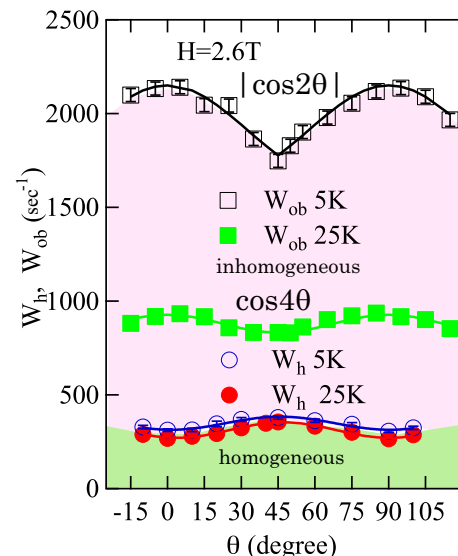

FIG. 11. Observed inhomogeneous Lorentzian W_{ob} (squares) and homogeneous Gaussian W_h (circles) linewidths in the paramagnetic (25 K) and HO (5 K) states in the same sample with RRR ~ 70. The W_{ob} are larger than the W_h as shown in Fig. 8. The peculiar $|\cos 2\theta|$ dependence due to MBCs is only observed in W_{ob} for the HO state [18–20]. Green and pink regions correspond to homogeneous and inhomogeneous contributions, respectively.

W_{ob} contribution due to the MBC is related with the static inhomogeneous Lorentzian envelope (e.g., Fig. 1) and has nothing to do with the homogeneous Gaussian echo decay effect. Likewise, the fourfold W_h width is derived entirely from the echo decay and has nothing at all to do with the static inhomogeneous broadening envelope. Fourfold symmetry remains in effect at 99% of U sites, consistent with the present observations. It is essential here that the fourfold homogeneous and twofold inhomogeneous broadenings have been separated using the spin-echo decay measurements.

W_{ob} increases in the HO state, whereas W_h is nearly the same. It appears that the inhomogeneous broadening is related to the HO [19]. Apart from the twofold contribution of the MBC to W_{ob}, there is a θ-independent contribution to W_{ob} that appears in the HO state as previously reported [24]. We note that the intrinsic nature of this effect is still unconfirmed, since it increases with decreasing sample quality. It should be noted that the peculiar coexistence of homogeneous fourfold and inhomogeneous twofold broadening is made observable by superior sample quality. In many cases, the inhomogeneous is much larger than the homogeneous broadening, owing to many different factors that smear out its angular dependence. Indeed, the θ-independent W_{ob} was so large (~ 6 times larger than in the present case [37]) in average quality URu_2Si_2 samples that the twofold effect is difficult to detect. In very pure single crystals of URu_2Si_2, however, MBC along [110] and [1$\bar{1}$0] are found to appear, whereupon their peculiar twofold broadening effect can be resolved. Ideally, in a perfect crystal, the twofold broadening would be expected to disappear, although no example of such a case has been reported. The complex nature of the twofold effect may explain the recent controversial observations regarding two and fourfold symmetry described in the Introduction. Recently, the nonlinear term of magnetic susceptibility that may reflect the twofold susceptibility is found to be sample-quality dependent [38].

Since the MBC effect is negligible in the paramagnetic state, this behavior seems to appear at the onset of the HO state. Perhaps the MBC effect is nearly degenerate with the HO state locally. Previous μSR measurements have indicated that a few percent of ordered magnetic centers appear in the HO state [39]; this may be related to the MBC broadening effect discussed above.

It is of interest to investigate the possibility of orthorhombic domain structure in the homogeneous broadening. If the twofold orthorhombic A and B domain states were to appear [8,18], the θ dependence of the spin-echo decay curves would be expressible as a superposition of decay curves for the two domains, which are rotated by 90° from each other in the basal plane. Thus,

$$\frac{m(2\tau)}{m(0)} \approx \frac{1}{2}\exp\left\{-\frac{1}{2}\left(\frac{2\tau}{T_{2G_A}}\right)^2\right\}$$
$$\times [(1 - f_{osc}) + f_{osc}\cos(G_A\tau)]$$
$$+ \frac{1}{2}\exp\left\{-\frac{1}{2}\left(\frac{2\tau}{T_{2G_B}}\right)^2\right\}$$
$$\times [(1 - f_{osc}) + f_{osc}\cos(G_B\tau)], \qquad (13)$$

with

$$\frac{1}{T_{2G_A}} = C_1 + C_2\cos 2\theta,$$
$$\frac{1}{T_{2G_B}} = C_1 + C_2\cos(2\theta + 180°) = C_1 - C_2\cos 2\theta,$$
$$G_A = D_1 + D_2\cos 2\theta,$$
$$G_B = D_1 + D_2\cos(2\theta + 180°) = D_1 - D_2\cos 2\theta,$$

where $C_{1,2}$ and $D_{1,2}$ are constants at a fixed temperature. If $C_2 \sim C_1$ and/or $D_2 \sim D_1$, curves of Eq. (13) would show multioscillation behaviors, which could not be fitted with unique T_{2G} and G, i.e., Eq. (11), whereas the observed curves can be well fitted with Eq. (11). If $C_1 \gg C_2$ and $D_1 \gg D_2$, Eq. (13) becomes effectively identical with Eq. (11) for $1/T_{2G} \cong (1/T_{2G_A} + 1/T_{2G_B})/2 = C_1$ and $G \cong (G_A + G_B)/2 = D_1$ due to a cancellation. Thus, there would be no θ dependence of $1/T_{2G}$ and G, whereas the fourfold $1/T_{2G} = W_h/0.47$ and G is observed.

In any case, the observed decay curves which are well fitted by Eq. (11) with fourfold G and $1/T_{2G}$ cannot be reproduced with the twofold two-domain description, although the $|\cos 2\theta|$ dependence of W_{ob} can be explained by either the twofold two-domain or the MBC descriptions [18–20].

B. Spatial range of the local fourfold electronic state

Based on the Van Vleck second moment theory [40], the expected homogeneous linewidth W_{hnn} due to the nn interactions is

$$W_{hnn} \sim \frac{9c}{8}\left|b + \gamma^2\hbar/r_{nn}^3\right| = 88 \text{ s}^{-1}, \qquad (14)$$

where $|b + \gamma^2\hbar/r_{nn}^3| = 148 \text{ s}^{-1}$ is the previously obtained value from measurements for $H \parallel$ [001] and [110] [25]. In the present case the observed $W_h \sim 350 \text{ s}^{-1}$ is larger than the calculated W_{hnn}, indicating that there are substantial contributions from beyond the first nn sites to the fourfold W_h, i.e., the Gaussian decay, whereas these contributions are not strong enough or sufficiently unique to cause multiple oscillation terms. In any case, the fourfold electronic state is concluded to extend at least well beyond nn sites, which is also consistent with the MBC description [20], while a precise estimation of fourfold range is difficult at the present.

As well as the fourfold region, it is difficult to estimate the twofold range surrounding an MBC quantitatively, however, it seems that the twofold regime is well localized around the MBC, which are $\sim 1\%$ of U sites.

VI. POSSIBLE SPACE GROUPS BASED ON GROUP THEORETICAL CONSIDERATIONS

In the present study, the fourfold rotational electronic local symmetry is confirmed at the Si and Ru sites in the HO state using a high quality single crystal sample. The homogeneous broadening Hamiltonian at the Si site [Eq. (2)] reflects the electronic state of the U site through RKKY [26] and PD [27] indirect spin-spin coupling processes that scatter heavy quasiparticles from filled to empty orbitals. Since nn U and Si sites are aligned along the c axis (see Fig. 4), fourfold

(C_4) electronic local symmetry at the U site is confirmed by fourfold broadening observations at the Si sites. Consequences from these observations will be discussed based on Landau's group theoretical treatment below.

Following a second-order phase transition, the lower symmetry of the ordered state belongs to one of the subgroups of the mother group (No. 139 $I4/mmm$) of the disordered (i.e., paramagnetic) state. Since breaking of time-reversal symmetry and crystal superlattice have not been confirmed in the HO state so far [5], there are 15 possible nonisomorphic (seven t and eight k) subgroups for the HO state: No. 69, 71, 87, 97, 107, 119, 121, 123, 126, 128, 129, 131, 134, 136, and 137 [7]. Among them, fourfold local symmetry for the U, Ru, and Si sites remains in No. 87: $I4/m$ with local symmetry (U: $4/m$, Ru: $\bar{4}$.., and Si: 4..) and No. 126: $P4/nnc$ with local symmetry (U: 422, Ru: $\bar{4}$.., and Si: 4..), which are two possible electronic space groups for the HO state. It should be noted that no lattice distortion is necessary to occur in the HO state for either case. As indicated by recent XRD measurements [12], the crystalline space group is considered to remain $I4/mmm$ in the HO state.

For the 4mm local symmetry at the Si site in the paramagnetic state, there should be mirror symmetry against (110) and (100) planes. In contrast, this mirror symmetry is not of necessity because of the 4.. local symmetry at the Si site in possible $I4/m$ and $P4/nnc$ cases for the HO state. It is remarkable that this symmetry appears to be preserved in the HO state within experimental error, considering the observed mirror symmetry of G and W_h against the [110] and [100] axes as shown in Figs. 7 and 8. This behavior of $1/T_{2G} = W_h/0.47$ and G can be understood as follows.

At the Si $(0,0,z)$ and $(1/2,1/2,z)$ sites ($z = 0.3724$ in URu$_2$Si$_2$ [21]), the symmetry axis in the basal plane can be assumed to deviate from the [110] axis (i.e., $\theta = 0°$) by angles δ and $-\delta$ for the $(0,0,z)$ and $(1/2,1/2,z)$ sites, respectively, in the $P4/nnc$ case, while by δ for both sites in the $I4/m$ case. In the $P4/nnc$ case, $1/T_{2G}$ and G can be specified approximately using a derivation similar to Eq. (13):

$$\frac{1}{T_{2G}} \sim C_1 + \frac{1}{2}C_2[\cos\{4(\theta + \delta)\} + \cos\{4(\theta - \delta)\}]$$
$$= C_1 + C_2\cos4\delta\cos4\theta,$$
$$G \sim D_1 + \frac{1}{2}D_2[\cos\{4(\theta + \delta)\} + \cos\{4(\theta - \delta)\}]$$
$$= D_1 + D_2\cos4\delta\cos4\theta, \qquad (15)$$

where relations $C_1 \gg C_2$ and $D_1 \gg D_2$ are satisfied in the present case. Thus, mirror symmetry appears to be preserved. Because two fourfold-tetragonal-domains with angle δ and $-\delta$ are formed in the $I4/m$ case, Eq. (15) can be adopted. Thus, mirror symmetry appears to be preserved again in the $I4/m$ case. Here δ seems to be small (i.e., $\cos4\delta \sim 1$) since the oscillation amplitude of $1/T_{2G}$ and G show no drastic change in the HO state (Figs. 7 and 8).

From the present study we cannot determine which electronic space group is relevant here. However, if the ordering wave vector is antiferromagnetic $Q = (001)$, as proposed in several measurements [41–43], No. 126: $P4/nnc$ can be selected, since doubling of the unit cell occurs for the No. 126
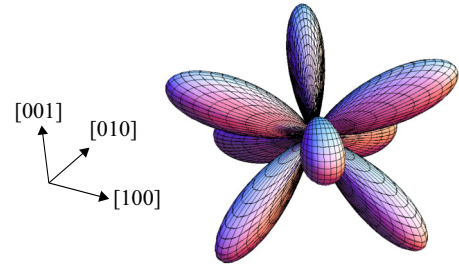

FIG. 12. Schematic electron distribution for A_{1u} (D_4) state. This type of ordering corresponds to electric dotriacontapolar order in the present case, which is a strong candidate for the HO state. The direction of the [100] (i.e., [010]) axis is midway between up and down lobes.

ordering case. On the other hand, No. 87: $I4/m$ is relevant for the ferromagnetic $Q = (000)$ case.

In the $P4/nnc$ case, the point group at the U site is 422 (D_4). An electronic state for the totally symmetric representation [44] of the 422 point group A_{1u}: $xyz(x^2 - y^2)$ (Fig. 12) cannot be composed entirely of U 5f orbitals because it is a rank 5 odd-parity multipole, i.e., electric dotriacontapole (see Table III of Ref. [45]). Therefore, the HO electronic state for the $P4/nnc$ case cannot be composed simply of U 5f states, but it is necessary to consider a contribution of U 6d orbitals as well. Much effort has been made to compose the relevant electronic state for the hidden-order parameter based on U 5f states alone. However, it is necessary to include the U 6d orbitals here to compose the real hidden-order electronic state. These somewhat unexpected aspects may be keys for identifying the hidden-ordered state. In contrast, the rank 4 even-parity multipole A_{2g}: $xy(x^2 - y^2)$ is expected for the $I4/m$ case, which can be composed of just U 5f orbitals [46,47].

An ordering of the A_{2g} state with $Q = (001)$ is proposed based on A_{2g}-type excitation observed in Raman spectroscopy [48,49], leading to the HO state No. 128: $P4/mnc$. However, this is unlikely since the fourfold symmetry at the Ru site is not preserved for $P4/mnc$. Compatibility between the A_{1u} ground state and the observed A_{2g}-type excitation in this itinerant electron system should also be carefully considered.

VII. CONCLUSION

The fourfold local electronic symmetry of the U, Ru, and Si sites has been confirmed in the hidden-order state of URu$_2$Si$_2$ by means of NMR measurements on a high-purity, single-crystal sample. At the Si site, the twofold line broadening is considered to be an extrinsic property due to imperfections in the crystal. Among possible subgroups of the mother paramagnetic space group $I4/mmm$, $I4/m$ and $P4/nnc$ are possible space groups for the HO state, which must satisfy the condition of U, Ru, and Si fourfold local electronic symmetries. These orderings are peculiar since none are accompanied by lattice distortion. Since $P4/nnc$ is the most likely candidate at the present, direct experimental identification of the A_{1u} rank 5 odd-parity multipole ordering (i.e., electric dotriacontapole) would be an important goal for future work.

APPENDIX

Figure 13 shows spin-echo decay results with different refocusing-pulse angles for $H = 2.52$ T $\parallel$ [001] axis at 25 K. The pulse amplitude is always large enough to uniformly excite the entire NMR line. As the refocusing pulse width decreases, the spin-echo decay weakens, indicating that the decay process is dominated by pulse modulation of static $I_{zi}I_{zj}$ couplings. The effect of the T_1 process is negligibly small. Thus, the echo is relaxed by the reorientation of neighbor spins caused by the refocusing pulse [28]. These measurements confirm that the echo decay is not affected by other dynamical processes, and that spin-spin couplings of the form $I_{\pm i}I_{\mp j}$ may be disregarded. In addition, if the spin-echo amplitude is
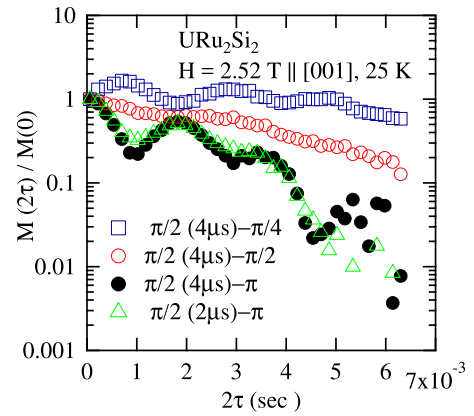

FIG. 13. Spin-echo decay curves for different refocusing (second) pulse widths for $H = 2.52$ T $\parallel$ [001] axis at 25 K. As the second pulse angle decreases, the spin-echo decay time becomes substantially longer, indicating that the spin-echo decay is driven exclusively by the rephasing pulse. The effect of the T_1 process is negligible. For the $\pi/2$-π pulse sequence, the echo decay curve is independent of the $\pi/2$ pulse width t_w ($4 \geqslant t_w \geqslant 2$ μs), under conditions where all nuclei are uniformly excited.

optimized with a $\pi/2$-π sequence, the spin-echo decay curve is independent of pulse intensity (Fig. 13).

[1] T. T. M. Palstra, A. A. Menovsky, J. van den Berg, A. J. Dirkmaat, P. H. Kes, G. J. Nieuwenhuys, and J. A. Mydosh, Superconducting and Magnetic Transitions in the Heavy-Fermion System URu$_2$Si$_2$, Phys. Rev. Lett. **55**, 2727 (1985).

[2] W. Schlabitz, J. Baumann, B. Pollit, U. Rauchschwalbe, H. M. Mayer, U. Ahlheim, and C. D. Bredl, Superconductivity and magnetic order in a strongly interacting fermi-system: URu$_2$Si$_2$, Z. Phys. B Condens. Matter **62**, 171 (1986).

[3] M. B. Maple, J. W. Chen, Y. Dalichaouch, T. Kohara, C. Rossel, M. S. Torikachvili, M. W. McElfresh, and J. D. Thompson, Partially Gapped Fermi Surface in the Heavy-Electron Superconductor URu$_2$Si$_2$, Phys. Rev. Lett. **56**, 185 (1986).

[4] V. Tripathi, P. Chandra, and P. Coleman, Heavy electrons: Sleuthing hidden order, Nat. Phys. **3**, 78 (2007).

[5] J. A. Mydosh and P. M. Oppeneer, Hidden order behaviour in URu$_2$Si$_2$ (A critical review of the status of hidden order in 2014), Philos. Mag. **94**, 3642 (2014).

[6] L. D. Landau and E. M. Lifshitz, *Statistical Physics Part 1* (Butterworth-Heinemann, Oxford, 1980).

[7] H. Harima, K. Miyake, and J. Flouquet, Why the hidden order in URu$_2$Si$_2$ is still hidden-one simple answer, J. Phys. Soc. Jpn. **79**, 033705 (2010).

[8] R. Okazaki, T. Shibauchi, H. J. Shi, Y. Haga, T. D. Matsuda, E. Yamamoto, Y. Onuki, H. Ikeda, and Y. Matsuda, Rotational symmetry breaking in the hidden-order phase of URu$_2$Si$_2$, Science **331**, 439 (2011).

[9] S. Tonegawa, K. Hashimoto, K. Ikada, Y.-H. Lin, H. Shishido, Y. Haga, T. D. Matsuda, E. Yamamoto, Y. Onuki, H. Ikeda, Y. Matsuda, and T. Shibauchi, Cyclotron Resonance in the Hidden-Order Phase of URu$_2$Si$_2$, Phys. Rev. Lett. **109**, 036401 (2012).

[10] S. C. Riggs, M. C. Shapiro, A. V. Maharaj, S. Raghu, E. D. Bauer, R. E. Baumbach, P. Giraldo-Gallo, M. Wartenbe, and I. R. Fisher, Evidence for a nematic component to the hidden-order parameter in URu$_2$Si$_2$ from differential elastoresistance measurements, Nat. Commun. **6**, 6425 (2015).

[11] S. Tonegawa, S. Kasahara, T. Fukuda, K. Sugimoto, N. Yasuda, Y. Tsuruhara, D. Watanabe, Y. Mizukami, Y. Haga, T. D. Matsuda, E. Yamamoto, Y. Onuki, H. Ikeda, Y. Matsuda, and T. Shibauchi, Direct observation of lattice symmetry breaking at the hidden-order transition in URu$_2$Si$_2$, Nat. Commun. **5**, 4188 (2014).

[12] C. Tabata, T. Inami, S. Michimura, M. Yokoyama, H. Hidaka, T. Yanagisawa, and H. Amitsuka, X-ray backscattering study of crystal lattice distortion in hidden order of URu$_2$Si$_2$, Philos. Mag. **94**, 3691 (2014).

[13] K. Kuwahara, H. Amitsuka, T. Sakakibara, O. Suzuki, S. Nakamura, T. Goto, M. Mihalik, A. A. Menovsky, A. deVisser, and J. J. M. Franse, Lattice instability and elastic response in the heavy fermion system URu$_2$Si$_2$, J. Phys. Soc. Jpn. **66**, 3251 (1997).

[14] C. Meingast and F. Hardy (private communication).

[15] K. Matsuda, Y. Kohori, and T. Kohara, Existence of line nodes in the superconducting energy gap of antiferromagnetic superconductor URu$_2$Si$_2$, J. Phys. Soc. Jpn. **65**, 679 (1996).

[16] S. Saitoh, S. Takagi, M. Yokoyama, and H. Amitsuka, ^{101}Ru NQR and hidden order in URu$_2$Si$_2$, J. Phys. Soc. Jpn. **74**, 2209 (2005).

[17] S. Takagi, S. Ishihara, M. Yokoyama, and H. Amitsuka, Symmetry of the hidden order in URu$_2$Si$_2$ from nuclear magnetic resonance studies, J. Phys. Soc. Jpn. **81**, 114710 (2012).

[18] S. Kambe, Y. Tokunaga, H. Sakai, T. D. Matsuda, Y. Haga, Z. Fisk, and R. E. Walstedt, NMR Study of In-Plane Twofold Ordering in URu$_2$Si$_2$, Phys. Rev. Lett. **110**, 246406 (2013).

[19] S. Kambe, Y. Tokunaga, H. Sakai, and R. E. Walstedt, Distributed twofold ordering in URu$_2$Si$_2$, Phys. Rev. B **91**, 035111 (2015).

[20] R. E. Walstedt, S. Kambe, Y. Tokunaga, and H. Sakai, Dilute RKKY model for NMR line broadening in the hidden-order state of URu$_2$Si$_2$, Phys. Rev. B **93**, 045122 (2016).

[21] T. D. Matsuda, E. Hassinger, D. Aoki, V. Taufour, G. Knebel, N. Tateiwa, E. Yamamoto, Y. Haga, Y. Onuki, Z. Fisk, and J. Flouquet, Details of sample dependence and transport properties of URu$_2$Si$_2$, J. Phys. Soc. Jpn. **80**, 114710 (2011).

[22] Y. Kohori, K. Matsuda, and T. Kohara, ^{29}Si NMR study of antiferromagnetic superconductor URu$_2$Si$_2$, J. Phys. Soc. Jpn. **65**, 1083 (1996).

[23] T. Hattori, H. Sakai, Y. Tokunaga, S. Kambe, T. D. Matsuda, and Y. Haga, No detectable change in in-plane ^{29}Si Knight shift in the superconducting state of URu$_2$Si$_2$, J. Phys. Soc. Jpn. **85**, 073711 (2016).

[24] S. Kambe, H. Sakai, Y. Tokunaga, T. Hattori, G. Lapertot, T. D. Matsuda, G. Knebel, J. Flouquet, and R. E. Walstedt, T Dependence of nuclear spin-echo decay at low temperatures in YbRh$_2$Si$_2$, Phys. Rev. B **95**, 195121 (2017).

[25] S. Kambe, T. Hattori, Y. Tokunaga, H. Sakai, T. D. Matsuda, Y. Haga, and R. E. Walstedt, Ruderman-Kittel interaction between Si in URu$_2$Si$_2$, J. Phys. Conf. Series **969**, 012033 (2018).

[26] M. A. Ruderman and C. Kittel, Indirect exchange coupling of nuclear magnetic moments by conduction electrons, Phys. Rev. **96**, 99 (1954).

[27] N. Bloembergen and T. J. Rowland, Nuclear spin exchange in solids: Tl^{203} and Tl^{205} magnetic resonance in thalliun and thallic oxide, Phys. Rev. **97**, 1679 (1955).

[28] R. E. Walstedt and S.-W. Cheong, ^{63,65}Cu and ^{17}O spin-echo decay and the static susceptibility $\chi'(q)$ in La$_{1.85}$Sr$_{0.15}$CuO$_4$, Phys. Rev. B **51**, 3163 (1995).

[29] H. Alloul and C. Froidevaux, Nuclear-magnetic-resonance spin echoes in alloys, Phys. Rev. **163**, 324 (1967).

[30] R. M. White, *Quantum Theory of Magnetism* (Springer, Berlin, 1983).

[31] G. Bastien, Interplay between magnetic quantum criticality, Fermi surface and unconvetional superconductivity in UCoGe, URhGe and URu$_2$Si$_2$, Doctoral thesis, University of Grenoble Alpes, 2017.

[32] M. M. Altarawneh, N. Harrison, G. Li, L. Balicas, P. H. Tobash, F. Ronning, and E. D. Bauer, Superconducting Pairs with Extreme Uniaxial Anisotropy in URu$_2$Si$_2$, Phys. Rev. Lett. **108**, 066407 (2012).

[33] T. Hattori, H. Sakai, Y. Tokunaga, S. Kambe, T. D. Matsuda, and Y. Haga, Evidence for Spin Singlet Pairing with Strong Uniaxial Anisotropy in URu$_2$Si$_2$ using Nuclear Magnetic Resonance, Phys. Rev. Lett. **120**, 027001 (2018).

[34] S. Takagi, S. Ishihara, S. Saitoh, H.-I. Sasaki, H. Tanida, M. Yokoyama, and H. Amitsuka, No evidence for "Small-Moment Antiferromagnetism" under ambient pressure in URu$_2$Si$_2$: Single-crystal ^{29}Si NMR study, J. Phys. Soc. Jpn. **76**, 033708 (2007).

[35] A. Abragam, *Principles of Nuclear Magnetism* (Clarendon, Oxford, 1961).

[36] R. E. Walstedt and L. R. Walker, Nuclear resonance line shapes due to magnetic impurities in metals, Phys. Rev. B **9**, 4857 (1974).

[37] O. O. Bernal, C. Rodrigues, A. Martinez, H. G. Lukefahr, D. E. MacLaughlin, A. A. Menovsky, and J. A. Mydosh, ^{29}Si NMR and Hidden Order in URu$_2$Si$_2$, Phys. Rev. Lett. **87**, 196402 (2001).

[38] M. Lawson, B. T. Bush, T. Kissikov, Z. Brubaker, K. R. Shirer, J. R. Jeffries, S. Ran, I. Jeon, M. B. Maple, and N. J. Curro, Measurements of the NMR knight shift tensor and nonlinear magnetization in URu$_2$Si$_2$, Phys. Rev. B **97**, 075138 (2018).

[39] H. Amitsuka, K. Tenya, M. Yokoyama, A. Schenck, D. Andreica, F. N. Gygax, A. Amato, Y. Miyako, Y. K. Huang, and J. A. Mydosh, Inhomogeneous magnetism in URu$_2$Si$_2$ studied by muon spin relaxation under high pressure, Physica B **326**, 418 (2003).

[40] J. H. Van Vleck, The dipolar broadening of magnetic resonance lines in crystals, Phys. Rev. **74**, 1168 (1948).

[41] E. Hassinger, G. Knebel, K. Izawa, P. Lejay, B. Salce, and J. Flouquet, Temperature-pressure phase diagram of URu$_2$Si$_2$ from resistivity measurements and ac calorimetry: Hidden order and Fermi-surface nesting, Phys. Rev. B **77**, 115117 (2008).

[42] A. Villaume, F. Bourdarot, E. Hassinger, S. Raymond, V. Taufour, D. Aoki, and J. Flouquet, Signature of hidden order in heavy fermion superconductor URu$_2$Si$_2$: Resonance at the wave vector $Q_0 = (1,0,0)$, Phys. Rev. B **78**, 012504 (2008).

[43] C. Bareille, F. L. Boariu, H. Schwab, P. Lejay, F. Reinert, and A. F. Santander-Syro, Momentum-resolved hidden-order gap reveals symmetry breaking and origin of entropy loss in URu$_2$Si$_2$, Nat. Commun. **5**, 4326 (2014).

[44] T. Inui, Y. Tanabe, and Y. Onodera, *Group Theory and Its Applications in Physics* (Springer, Berlin, 1990).

[45] S. Hayami and H. Kusunose, Microscopic description of electric and magnetic toroidal multipoles in hybrid orbitals, J. Phys. Soc. Jpn. **87**, 033709 (2018).

[46] H. Kusunose and H. Harima, On the hidden order in URu$_2$Si$_2$-antiferro hexadecapole order and its consequences, J. Phys. Soc. Jpn. **80**, 084702 (2011).

[47] K. Haule and G. Kotliar, Arrested Kondo effect and hidden order in URu$_2$Si$_2$, Nat. Phys. **5**, 796 (2009).

[48] J. Buhot, M.-A. Méasson, Y. Gallais, M. Cazayous, A. Sacuto, G. Lapertot, and D. Aoki, Symmetry of the Excitations in the Hidden Order State of URu$_2$Si$_2$, Phys. Rev. Lett. **113**, 266405 (2014).

[49] H.-H. Kung, R. E. Baumbach, E. D. Bauer, V. K. Thorsmolle, W.-L. Zhang, K. Haule, J. A. Mydosh, and G. Blumberg, Chirality density wave of the "Hidden Order" phase in URu$_2$Si$_2$, Science **347**, 1339 (2015).